Influences of anionic and cationic dopants on the morphology and optical properties of PbS nanostructures

Ramin Yousefi[a)†], Mohsen Cheragizade[b)], Farid Jamali-Sheini[c)], M. R. Mahmoudian[d)], Abdolhossein Saaédi[b)], and Nay Ming Huang[e)]

[a)] *Department of Physics, Masjed-Soleiman Branch, Islamic Azad University (I.A.U.), Masjed-Soleiman, Iran*
[b)] *Department of Electrical Engineering, Bushehr Branch, Islamic Azad University (I.A.U.), Bushehr, Iran*
[c)] *Department of Physics, Ahwaz Branch, Islamic Azad University, Ahwaz, Iran*
[d)] *Department of Chemistry, Shahid Sherafat, University of Farhangian,* 15916 *Tehran, Iran*
[e)] *Low Dimensional Materials Research Center, Department of Physics, Faculty of Science, University of Malaya,* 50603 *Kuala Lumpur, Malaysia*

(Received 15 January 2014; revised manuscript received 20 April 2014; published online 20 August 2014)

Selenium and zinc are used as anionic and cationic dopant elements to dope PbS nanostructures. The undoped and doped PbS nanostructures are grown using a thermal evaporation method. Scanning electron microscopy (SEM) results show similar morphologies for the undoped and doped PbS nanostructures. X-ray diffraction (XRD) patterns of three sets of the nanostructures indicate that these nanostructures each have a PbS structure with a cubic phase. Evidence of dopant incorporation is demonstrated by X-ray photoelectron spectroscopy (XPS). Raman spectra of the synthesized samples confirm the XRD results and indicate five Raman active modes, which relate to the PbS cubic phase for all the nanostructures. Room temperature photoluminescence (PL) and UV–Vis spectrometers are used to study optical properties of the undoped and doped PbS nanostructures. Optical characterization shows that emission and absorption peaks are in the infrared (IR) region of the electromagnetic spectrum for all PbS nanostructures. In addition, the optical studies of the doped PbS nanostructures reveal that the band gap of the Se-doped PbS is smaller, and the band gap of the Zn-doped PbS is bigger than the band gap of the undoped PbS nanostructures.

Keywords: PbS nanostructures, anionic dopant, cationic dopant, thermal evaporation, optical properties

PACS: 81.15.Gh, 61.72.uf, 61.72.uj, 78.55.−m **DOI:** 10.1088/1674-1056/23/10/108101

1. Introduction

Metal chalcogenide semiconductors have attracted much attention because of their potential applications. In fact, nanocrystals of semiconducting metal chalcogenides (II–VI and IV–VI) are the materials that exhibit band gap energies spanning from the mid-to-near infrared (PbS, PbSe, PbTe) to the visible (CdS, CdSe, CdTe), and into the ultraviolet (ZnS, ZnSe) regions.

Among metal chalcogenides, lead sulfide (PbS) is a semiconductor with a narrow band gap of 0.41 eV and a large exciton Bohr radius of 18 nm, which permits size-quantum confinement effects to be clearly visible, even for larger particles.[1] Therefore, growth of PbS nanostructures of different sizes can result in obtaining different applications for this important semiconductor. In fact, it has important optical applications, such as solar cells and infrared detectors,[2] solar control coatings optical fibers,[3] and broadband optical amplifiers.[4] As is well known, impurity doping in semiconductors with selective elements greatly affects the basic physical properties (electrical, optical, and magnetic), which are crucial for their practical application. Many researchers have reported the synthesis of doped PbS nanoparticles, films, and one-dimensional (1D) nanostructures, and have also studied the electrical, optical, and magnetic properties of these doped nanostructures.[5–11]

Generally, selective elements such as dopant materials in PbS can be classified as two groups of materials: one group can be substituted for Pb, and the other can be substituted for S. These different types of doping materials can exhibit different optical properties from those of PbS, owing to the different treatments of Pb and S in the PbS structure. Zn as a cation dopant and Se as an anion dopant can be substituted for Pb and S, respectively. Both elements can be used as impurities that change the band gap of PbS. He *et al.* reported Zn-doped PbS quantum dots, which were synthesized by a wet chemical method.[12] They showed that Zn as a dopant material can affect the optical band gap of PbS nanostructures. Therefore, a comparison of the optical behavior between these two types of doping materials in PbS can help us to carry out band gap engineering for PbS nanostructures.

In this work, undoped, Se-doped, and Zn-doped PbS nanostructures are grown by a thermal evaporation method. Then, a comparison of optical behavior between the doped and undoped PbS nanostructures is carried out by photoluminescence and UV–Vis spectroscopy.

†Corresponding author. E-mail: yousefi.ramin@gmail.com, raminyousefi@iaumis.ac.ir

© 2014 Chinese Physical Society and IOP Publishing Ltd

2. Experiment

The growth of the undoped and doped PbS nanostructures was performed in a horizontal tube furnace on Si (111) substrates. High-purity lead sulfide powder (99.99%) was used as the precursor material to grow the undoped PbS nanostructures. The precursor material was placed in a small quartz tube and an Si (111) substrate was placed downstream of the precursor material. The small tube was then inserted into a vacuum chamber so that the precursor material was at the center of the furnace. The precursor material and silicon substrate were heated to 700 °C and 400 °C, respectively. High-purity Ar (90%)/H_2(10%) gas was fed at a rate of about 25 sccm into the furnace at one end, while the other end was connected to a rotary pump. The growth process lasted 1 h. A vacuum of 15 Torr (1 Torr $= 1.33322 \times 10^2$ Pa) was maintained inside the tube furnace during the deposition of the nanostructures. The same conditions were used to grow the doped-PbS nanostructures. Material dopants (high-purity Se and Zn powders) were placed upstream of the PbS powder at different temperatures. The details of the experimental set-up for growing these samples are shown in Fig. 1.

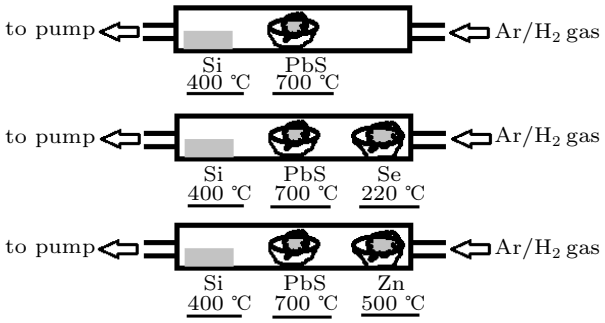


Fig. 1. Schematics of the set-ups for growth of undoped, Se-, and Zn-doped PbS nanostructures.

The morphologies and crystal structures of the products were investigated using a field emission scanning electron microscope (FESEM; Hitachi S4160) and an X-ray diffractometer (XRD; Siefert ID 3003). Elemental analyses of the products were undertaken using X-ray photoelectron spectroscopy (XPS; VG-Microtech ESCA-2000). The XPS spectra were recorded using Mg–K_α radiation (1256.6 eV). Room temperature photoluminescence (Jobin Yvon Horiba HR 800 UV), UV–Vis (Lambda 25-Perkin–Elmer) and Raman (Bruker–Senterra Raman Spectrometer) spectrometers were employed to study the optical properties and crystallinities of the PbS nanostructures, respectively. An Nd:YLF laser with a wavelength of 785 nm and an He–Cd laser with a wavelength of 325 nm were used for Raman and PL measurements, respectively.

3. Results and discussion

Figure 2 shows the FESEM images and the EDX spectra of the undoped, Se-, and Zn-doped PbS nanostructures. Figure 2(a) shows a star morphology for the undoped PbS nanostructures with an average grain diameter of about 90 nm. It can be seen that the Se-doped PbS nanostructure has a similar morphology to the undoped PbS nanostars (Fig. 2(b)). However, the faces of the Se-doped PbS nanostars are flat. In addition, the sizes of the Se-doped PbS nanostars are bigger than those of the undoped-PbS nanostars. Figure 2(c) shows the FESEM image of the Zn-doped PbS nanostructures. The image reveals a spherical shape for the Zn-doped nanostructures, of a similar size to the shape for the undoped-PbS nanostars. Figure 2(d) shows an EDX spectrum of the undoped PbS nanostars. The spectrum indicates that the nanostars are pure PbS. Figures 2(e) and 2(f) show the EDX spectra of the doped PbS nanostructures. The EDX spectra of the Se- (Fig. 2(e)) and Zn-doped (Fig. 2(f)) structures indicate different percentages of selenium and zinc, i.e., 3.4% (atm), and 1.1% (atm), respectively. In addition, the EDX spectra reveal the peaks from the Si substrate and oxygen. The oxygen peak could be a result of a leakage of the set-up, or from the Si substrate. It is known that oxygen as a defect usually appears in the PbS structures.

Figure 3(a) shows the XRD patterns of the undoped and doped PbS nanostructures. The obtained XRD patterns are in good agreement with the data on the standard card of bulk PbS with an fcc phase (JCDPDS Card No. 05-0592). There are no other peaks related to PbSe, ZnS, PbO, ZnO, or other mixed compounds. The ionic radius of the substituted Zn^{2+} (0.74 Å) is smaller than that of Pb^{2+} (1.19 Å), and the ionic radius of the substituted Se^{2-} (0.5 Å) is bigger than that of S^{2-} (0.37 Å). Thus, Zn doping causes the XRD peaks to slightly shift toward higher diffraction angles, while the Se doping induces the XRD peaks to slightly shift toward lower diffraction angles than the undoped PbS (Fig. 3(b)). These results provide indirect evidence that zinc and selenium are incorporated into the crystal structure of PbS.

The further evidence for the formation of PbS, Se-doped PbS, and Zn-doped PbS in the present system comes from XPS analysis of the products. Figure 4 shows the high-resolution XPS spectra of the products. Figures 4(a) and 4(b) show the binding energies of Pb $4f_{7/2}$, Pb $4f_{5/2}$, and S $2p_{3/2}$ for the undoped-PbS nanostructures at 139.08, 144.08, and 161.44 eV, respectively, which are very close to the values reported in our previous work.[13] Figures 4(c) and 4(e) reveal the binding energies of Pb $4f_{7/2}$, Pb $4f_{5/2}$, S $2p_{3/2}$, and Se 3d for the Se-doped PbS nanostructures at 139.11, 144.11, 161.03, and 53.8 eV, respectively. It can be seen that the S concentration decreases due to the occurrence of Se in the PbS structure.

The XPS spectra of Zn-doped PbS nanostructures are shown in Figs. 4(f)–4(h). The peaks at 139.25, 144.25, 161.66, 1021.9, and 1045 eV belong to the binding energies of Pb $4f_{7/2}$, Pb $4f_{5/2}$, S $2p_{3/2}$, Zn $2p_{3/2}$, and Zn $2p_{1/2}$, respectively. The slight shift in the peaks can be ascribed to the effect of changes in binding energy due to the strain-induced distortion of the PbS lattice. In addition, the percentage molar concentrations of the Se and Zn doped into Se-doped and Zn-doped PbS nanostructures are calculated to be 3.1 and 1.2, respectively. In fact, the XPS results confirm the presence of Se and

Zn in the PbS structure. Deconvolution of the overall region indicates that the binding energies of Se and Zn are associated with Pb–Se and Zn–S bands as closely referenced to PbSe[14] and ZnS.[15]

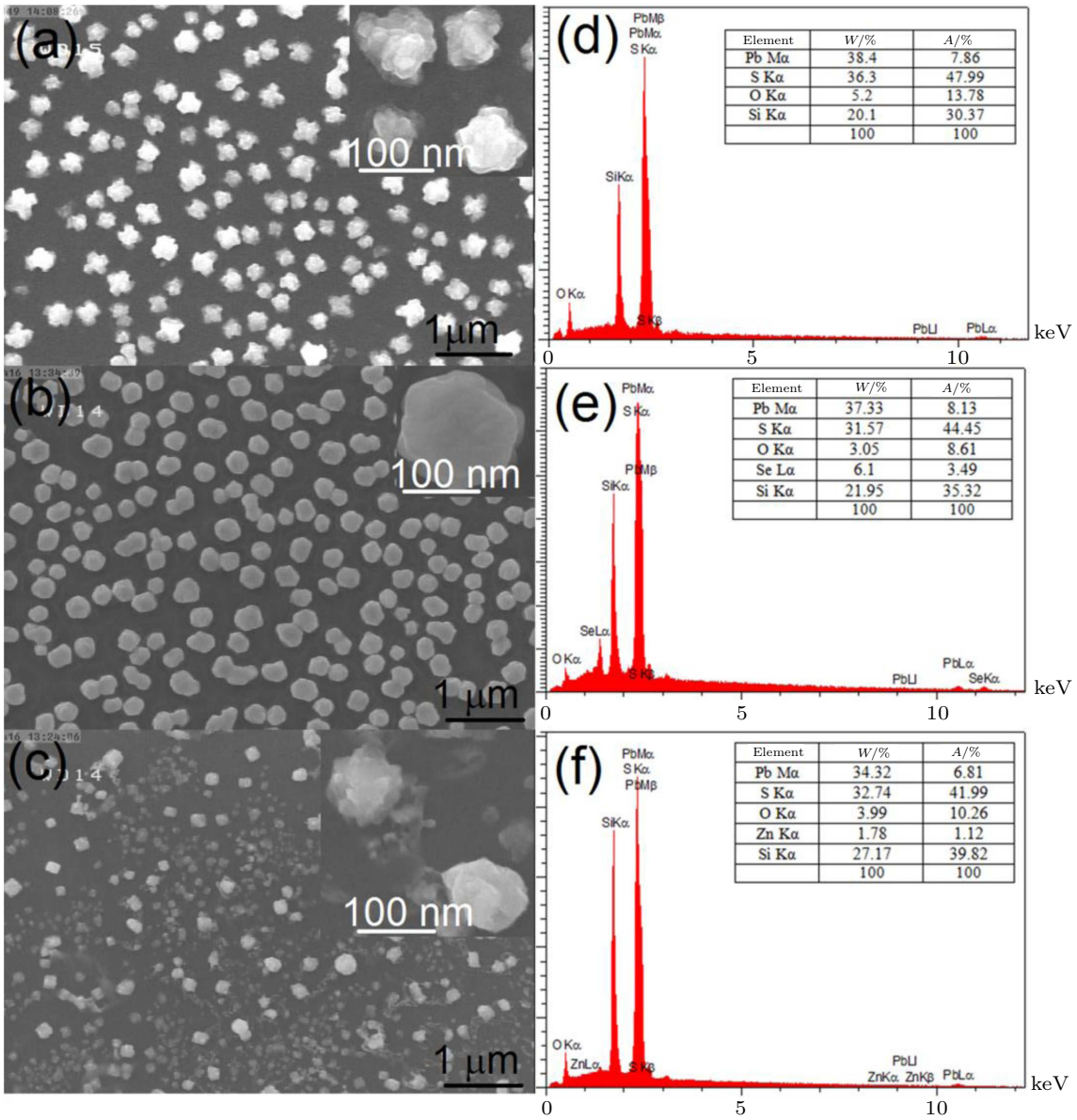


Fig. 2. (color online) FESEM images of (a) the undoped-, (b) Se-doped, and (c) Zn-doped PbS nanostructures, and EDX spectra of (d) the undoped, (e) Se-doped, and (f) Zn-doped PbS nanostructures.

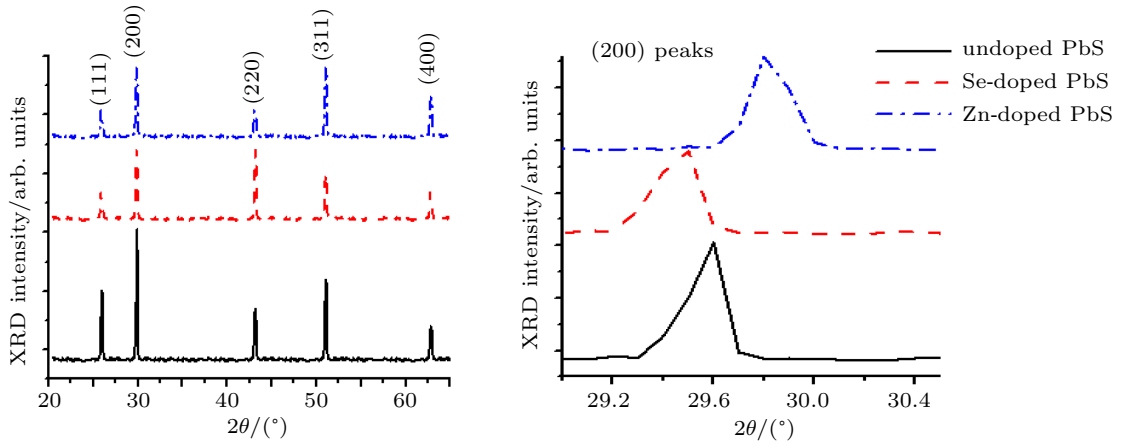


Fig. 3. (color online) (a) XRD patterns of the undoped- and doped-PbS nanostructures with cubic phase, and (b) the shifts in the (200) peak of the undoped, Se-, and Zn-doped PbS nanostructures.

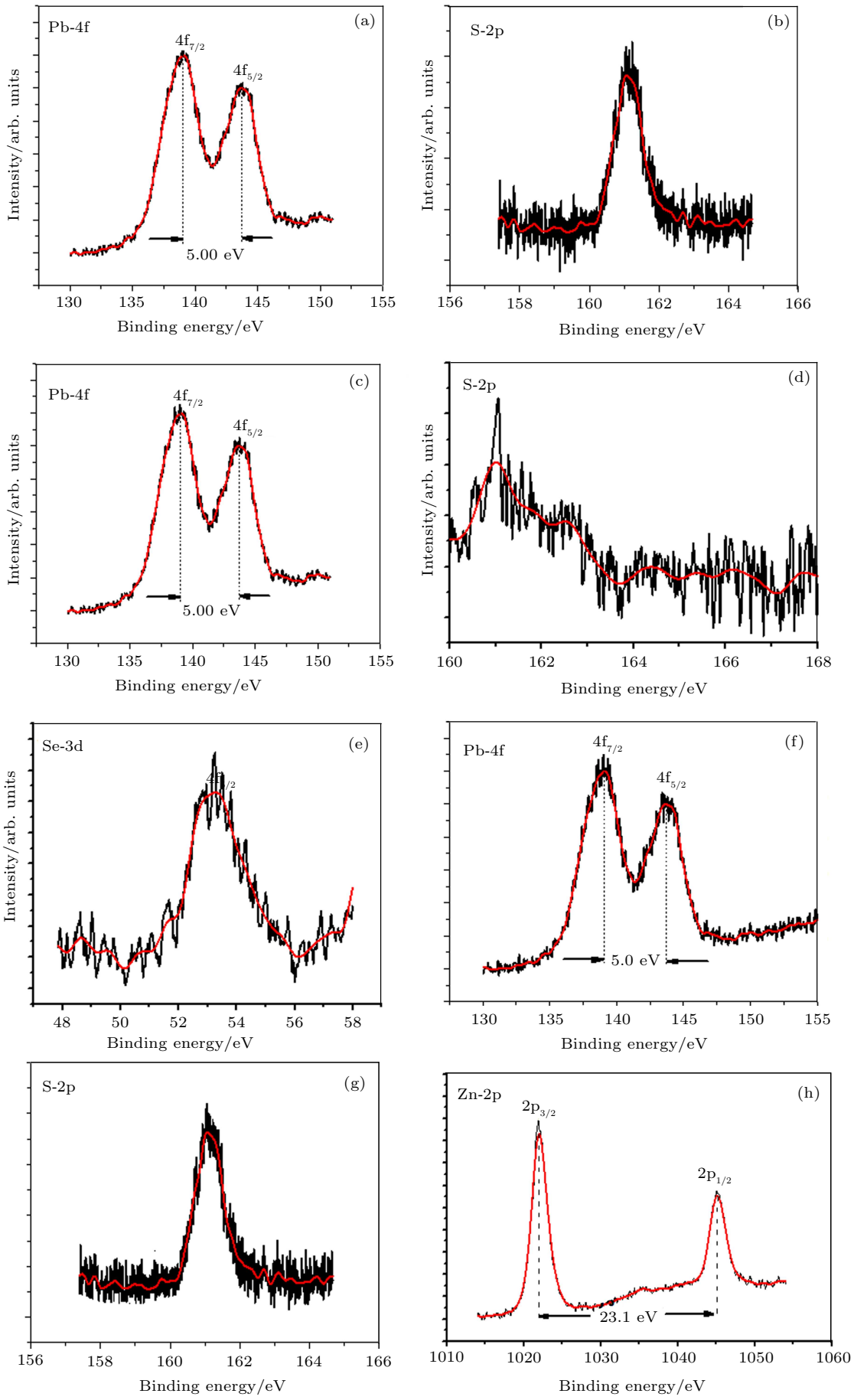


Fig. 4. (color online) XPS spectra of the ((a) and (b)) undoped PbS nanostructures, ((c) and (e)) Se-doped PbS nanostructures, and ((f)–(h)) Zn-doped PbS nanostructures.

Based on these results, the plausible growth mechanism of the PbS nanostars can be explained by the following CVD reactions:

$$\mathrm{PbS(s)} \rightarrow \mathrm{PbS(g)}, \quad (1)$$

$$\mathrm{PbS(g)} + \mathrm{H_2(g)} \rightarrow \mathrm{Pb(g)} + \mathrm{H_2S(g)} \ \text{(in source position)}, \quad (2)$$

$$\mathrm{Pb(g)} \rightarrow \mathrm{Pb(l)} \rightarrow \mathrm{Pb(s)}$$

(the deposited Pb(s) can act as seed on the substrate), (3)

$$\mathrm{Pb(s)_{deposited}} + \mathrm{H_2S(g)} \rightarrow \mathrm{PbS(s)} + \mathrm{H_2(g)}$$

(the size and shape of PbS dictated by deposited Pb(s)). (4)

In fact, the H_2 gas plays a catalyst role in the growth process of the PbS nanostars. To better understand the details of Pb(s) formation on the Si substrate, the above experiment under the same conditions is repeated for 10 minutes. Then, the obtained sample is characterized by the XRD. This XRD pattern is shown in Fig. 5. It can be seen that the pattern indicates only Pb and Si peaks. Reaction (3) shows that the Pb gas is thus transported downstream and condensed into liquid droplets on the substrate. In the next step, the liquid Pb acts as a preferential adsorption site for PbS, which can be formed in the reverse reaction of the gaseous Pb and H_2S, or in the progressive *in-situ* conversion of the liquid Pb from exposure to H_2S (reaction (4)). Alloys Pb and PbS are thus created while the adsorption proceeds, followed by nucleation and subsequent uni-dimensional crystallization, which can occur in the liquid–solid interface once supersaturation is reached.

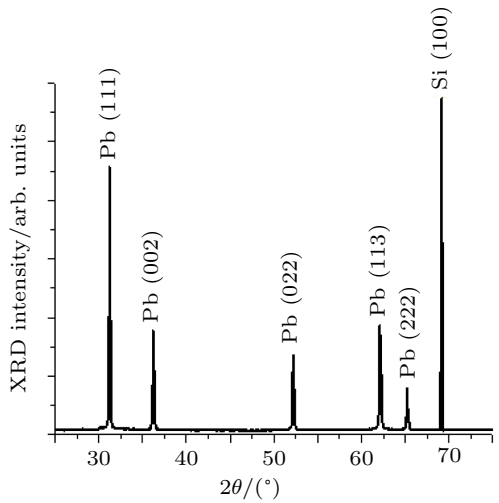


Fig. 5. XRD pattern of the sample after 10-min deposition.

Based on the growth reactions of PbS in the presence of H_2 gas, and according to the XRD and EDX results, the possible reactions for the doping of Se and Zn can be written as the following CVD reactions:

a) Se-doped PbS

$$\mathrm{Se(s)} \rightarrow \mathrm{Se(l)} \rightarrow \mathrm{Se(g)}, \quad (5)$$

$$\mathrm{PbS(s)} \rightarrow \mathrm{PbS(g)}, \quad (6)$$

$$\mathrm{PbS(g)} + x\mathrm{Se(g)} \rightarrow \mathrm{PbS_{(1-x)}Se_x(g)} + x\mathrm{S(g)}, \quad (7)$$

$$\mathrm{PbS_{(1-x)}Se_x(g)} + \mathrm{H_2(g)} \rightarrow \mathrm{Pb(g)} + (1-x)\mathrm{H_2S(g)} + x\mathrm{H_2Se}, \quad (8)$$

$$\mathrm{Pb(g)} \rightarrow \mathrm{Pb(l)} \rightarrow \mathrm{Pb(s)}$$

(the deposited Pb(s) can act as seed on the substrate), (9)

$$\mathrm{Pb(s)_{deposited}} + (1-x)\mathrm{H_2S(g)} + x\mathrm{H_2Se(g)} \rightarrow \mathrm{PbS_{(1-x)}Se_x(s)} + \mathrm{H_2(g)}; \quad (10)$$

b) Zn-doped PbS

$$\mathrm{Zn(s)} \rightarrow \mathrm{Zn(l)} \rightarrow \mathrm{Zn(g)}, \quad (11)$$

$$\mathrm{PbS(s)} \rightarrow \mathrm{PbS(g)}, \quad (12)$$

$$\mathrm{PbS(g)} + x\mathrm{Zn(g)} \rightarrow \mathrm{Pb_{(1-x)}Zn_xS\ (g)} + x\mathrm{Pb\ (g)}, \quad (13)$$

$$\mathrm{Pb_{(1-x)}Zn_xS(g)} + \mathrm{H_2(g)} \rightarrow \mathrm{Pb_{(1-x)}Zn_x(g)} + \mathrm{H_2S(g)}, \quad (14)$$

$$\mathrm{Pb_{(1-x)}Zn_x(g)} \rightarrow \mathrm{Pb_{(1-x)}Zn_x(l)} \rightarrow \mathrm{Pb_{(1-x)}Zn_x(s)}$$

(the size and shape of $\mathrm{Pb_{(1-x)}Zn(s)S}$ dictated by deposited $\mathrm{Pb_{(1-x)}Zn_x(s)}$), (15)

$$\mathrm{Pb_{(1-x)}Zn_x(s)_{deposited}} + \mathrm{H_2S(g)} \rightarrow \mathrm{Pb_{(1-x)}Zn_xS(s)} + \mathrm{H_2(g)}$$

(the size and shape of $\mathrm{Pb_{(1-x)}Zn_x(s)S}$ dictated by deposited $\mathrm{Pb_{(1-x)}Zn(s)}$). (16)

As can be seen from reaction (16), the size of $\mathrm{Pb_{(1-x)}Zn_xS}$ is dictated by the deposited $\mathrm{Pb_{(1-x)}Zn_x(s)}$. The comparison of this reaction with similar reactions from the deposition of the undoped PbS and $\mathrm{PbS_{(1-x)}Se_x}$ can help us make the following conclusion: by changing the type of the deposited seed, the shape of doped PbS can be changed. The FESEM images confirm these results.

Raman spectroscopy is an effective technique for estimating the crystallinity of a material. It is well known that in a crystalline semiconductor the observed Raman shifts usually correspond to the longitudinal optical phonons (LO), whereas other modes, such as transverse optical phonons (TO) and surface phonons (SP), are, in general, not observable because of symmetry restrictions and low intensities, respectively. However, as the surface-to-volume ratio is large for nanostructured materials, it is possible to observe the SP mode by Raman scattering measurements.[16] According to group theory, single crystalline PbS belongs to the $Fm3m$ space group. Figure 6 shows the Raman spectra of the PbS nanostructures. The spectra of Fig. 6 contain bands at 252, 305, 435, 621, and 943 $\mathrm{cm^{-1}}$. All of these modes belong to the PbS structure with a cubic phase. It can be seen that the peak at 252 $\mathrm{cm^{-1}}$ in Se-doped PbS has a stronger intensity than in the undoped and Zn-doped PbS nanostructures. The peak at 252 $\mathrm{cm^{-1}}$ corresponds to an SP mode that could appear due to the surface roughness of deposited material.[16] In fact, this result could be a consequence of the different treatments of Pb and S in the PbS structure. However, more studies are needed to explain

this phenomenon in the future. The Raman peak at 434 cm^{-1} is attributed to the first overtone (2LO).[17] The band centered at 970 cm^{-1} may be attributed to sulfates in the sample, owing to laser-induced degradation.[18]

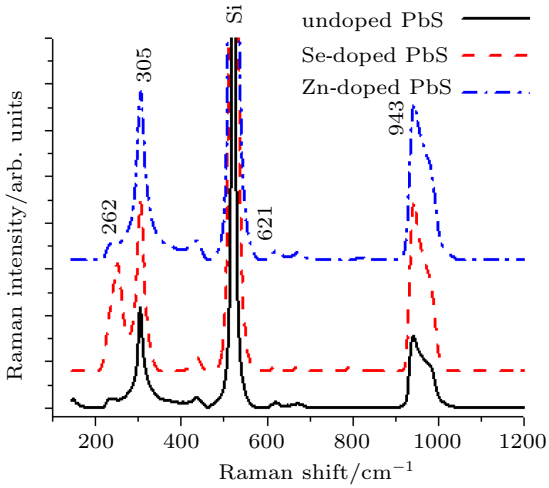


Fig. 6. (color online) Raman spectra of the undoped and doped PbS nanostructures with cubic phase.

The UV–Vis absorbance spectra of the PbS nanostructures are shown in Fig. 7(a). The relevant decrease in the absorbance at wavelengths greater than 800 nm can be also assigned to the intrinsic band gap absorbance of PbS, owing to the electron transitions from the valence band to the conduction band. It can be observed that the absorbance intensity of the Se-doped PbS nanostructures is smaller than that of the Zn-doped PbS nanostructures. The direct band gap can be estimated from the maximum of the curve for the first derivative of the absorbance versus energy and from the intersection of the second derivative with the energy axis.[19] Figures 7(b)–7(d) show these results of the band gap energies of the undoped and doped PbS nanostructures. It can be seen that the band gaps of the Se-doped PbS nanostructures are smaller than those of the undoped PbS nanostructures, while the band gaps of the Zn-doped PbS nanostructures are bigger than those of the undoped PbS nanostructures. In addition, the samples are characterized by a PL spectrometer. The PL emission and excitation spectra are directly related to the optical transitions contributing to the light emission process. Therefore, it is one of the most sensitive methods of investigating electronic levels. Figure 7(e) shows the PL spectra of the PbS nanostructures. It can be seen that peaks at 749 nm (1.65 eV), 782 nm (1.58 eV), and 806 nm (1.53 eV) are for the Zn-doped, undoped, and Se-doped PbS

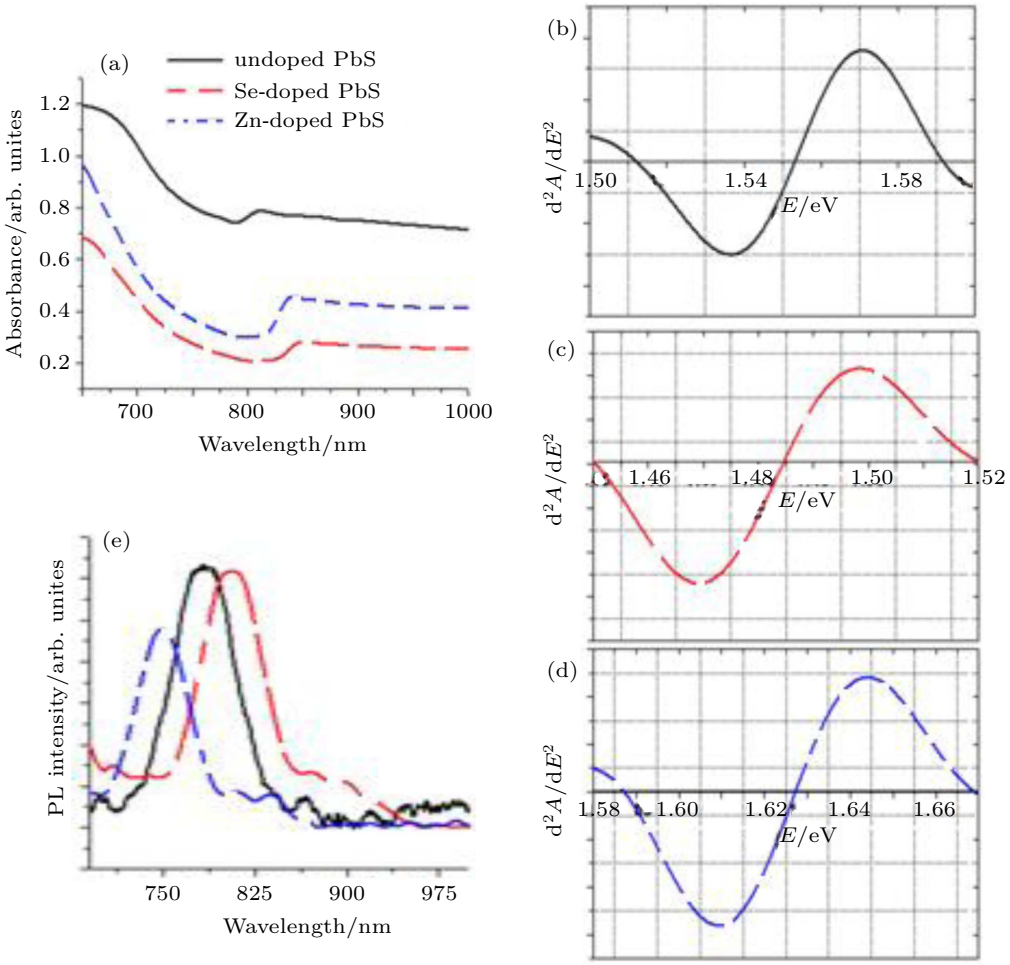


Fig. 7. (color online) (a) Absorbance spectra of the undoped and doped PbS nanostructures; (b)–(d) exact band gaps of the PbS nanostructures by the second derivative and energy axle intersect; (e) PL spectra of the undoped and doped PbS nanostructures.

nanostructures, respectively. The PL peak at around 749 nm–806 nm in wavelength is associated with the transition of electrons from the conduction band edge to holes trapped at interstitial Pb^{2+} sites.[20]

In fact, the alloying of PbS with ZnS and PbSe creates a $Pb_{(1-x)}Zn_xS$ and $PbS_{(1-x)}Se_x$ structure. ZnS and PbSe, which have a larger (3.54 eV) and smaller (0.28 eV) band gap than PbS, can result in a widened and narrowed band gap of PbS, respectively. It can be seen that the PL and UV–Vis results show the same results for the band gap of the PbS nanostructures, approximately. In fact, these results show that the band gaps of the undoped and doped PbS nanostructures are in the shortwave infrared (SWIR) region.

4. Conclusions

A comparative study is carried out between Se as an anionic and Zn as a cationic dopant of the doped PbS nanostructures, which are grown using a simple thermal evaporation set-up. FESEM images show that the morphologies of the undoped and doped PbS nanostructures are similar. The XRD and XPS results indicate that the Zn and Se exist in the PbS nanostructures. Raman results reveal the same vibration behaviors for all the samples, except an SP mode that appears in the Se-doped PbS nanostructures. Optical characterization indicates that the band gaps of the PbS nanostructures are widened and narrowed by a cationic and anionic dopant respectively. Furthermore, these results show that the band gaps of the undoped and doped PbS nanostructures are in the SWIR region. Therefore, these samples could be used as SWIR detectors or sources with different wavelengths, in this region of the electromagnetic spectrum.

Acknowledgment

R. Yousefi is grateful to the Iranian National Science Foundation (INSF) for a research grant support. R. Yousefi and F. Jamali-Sheini thank the Islamic Azad University (I.A.U.), Masjed-Soleiman and Ahwaz Branches, respectively, for their financial support of this research work. In addition, N. M. Huang thanks the financial support from the Ministry of Higher Education of Malaysia for the High Impact Research Grant (UM.C/1/HIR/MOHE/SC/21).

References

[1] Bakueva L, Konstantatos G, Levina L, Musikhin S and Sargent E H 2004 *Appl. Phys. Lett.* **84** 3459
[2] Ortuno-Lopez M B, Valenzuela-Jauregui J J, Ramirez-Bon R, Prokhorov E and Gonzalez-Hernandez J 2002 *J. Phys. Chem. Solids* **63** 665
[3] Kumar S, Sharma T P, Zulfequar M and Husain M 2003 *Physica B* **325** 8
[4] Liu C, Heo J, Zhang X and Adam J L 2008 *J. Non-Cryst. Solids* **354** 618
[5] Wei H, Chen S, Ren X, Qian B, Su Y, Yang Z and Zhang Y 2012 *Cryst. Eng. Comm.* **14** 7408
[6] Rajen Singh L, Bobby Singh S and Rahman A 2013 *Chalcogenide Letters* **10** 167
[7] He X, Demchenko I N, Stolte W C, Van Buuren A and Liang H 2012 *J. Phys. Chem. C* **116** 22001
[8] He J, Blum I D, Wang H Q, Girard S N, Doak J, Zhao LD, Zheng J C, Casillas G, Wolverton C, Jose-Yacaman M, Seidman D N, Kanatzidis M G and Dravid V P 2012 *Nano Lett.* **12** 5979
[9] Long G, Barman B, Delikanli S, Tsai Y T, Zhang P, Petrou A and Zeng H 2012 *Appl. Phys. Lett.* **101** 062410
[10] Das R and Kumar R 2012 *Mater. Res. Bull.* **47** 239
[11] Thangavel S, Ganesan S and Saravanan K 2012 *Thin Solid Films* **520** 5206
[12] He X, Demchenko I N, Stolte W C, Buuren A V and Liang H 2012 *Phys. Chem. C* **116** 22001
[13] Cheraghizade M, Yousefi R, Jamali-Sheini F, Saáedi A and Huang N M 2014 *Mat. Sci. Semicond. Proc.* **21** 98
[14] Law M, Luther J M, Song Q, Hughes B K, Perkins C L and Nozik A J 2008 *J. Am. Chem. Soc.* **130** 5974
[15] Laihia R, Leiro J A, Kokko K and Mansikka K 1996 *J. Phys.: Condens. Matter* **8** 6791
[16] Ge J P, Wang J, Zhang H X, Wang X, Peng Q and Li Y D 2005 *Chem. Eur. J.* **11** 1889
[17] Smith G D, Firth S, Clark R J H and Cardona M 2002 *J. Appl. Phys.* **92** 4375
[18] Xiong S, Xi B, Xu D, Wang C, Feng X, Zhou H and Qian Y 2007 *J. Phys. Chem. C* **111** 16761
[19] Khorsand Zak A, Abd Majid W H, Mahmoudian M R, Darroudi M and Yousefi R 2013 *Adv. Powder Technol.* **24** 618
[20] Cao H, Wang G, Zhang S and Zhang X 2006 *Nanotechnology* **17** 3280